Entropic broadening of the spin-crossover pressure in ferropericlase

Kaishuai Yang,[1,2] Xianlong Wang,[1,2,*] Jie Zhang,[1,2] Ya Cheng,[1,2] Chuanguo Zhang,[1] Zhi Zeng,[1,2,3,†] and Haiqing Lin[3]

[1]*Key Laboratory of Materials Physics, Institute of Solid State Physics, HFIPS, Chinese Academy of Sciences, Hefei 230031, China*

[2]*University of Science and Technology of China, Hefei 230026, China*

[3]*Beijing Computational Science Research Center, Beijing 100084, China*

(Received 19 June 2018; revised 26 May 2021; accepted 8 June 2021; published 23 June 2021)

The pressure-induced spin crossover of iron in ferropericlase, the Fe-bearing MgO, is a key to understanding the seismological observations in the lower mantle. However, the experimentally measured spin-crossover pressure zone (SCPZ) shows large variations, which disagree with the theoretically predicted values that are generally less than half of experimental ones. Here, we resolve this outstanding controversy by revealing the critical role of Fe distribution in MgO in broadening the Fe SCPZ, using comprehensive first-principles calculations combined with cluster expansion approach and Monte Carlo simulations. By employing a large supercell containing up to $\sim 10^6$ atoms, we derive the spin-crossover pressures as functions of Fe concentration for different Fe distributions. We determine a critical temperature of $T_c \sim 900$ K, below which Fe segregation (clustering) occurs, in accordance with the thermodynamic phase diagram. Above T_c, an entropy-driven randomized Fe distribution creates large variations in Fe local environments, which in turn broadens the SCPZ, such as 17.5 GPa for 25 mol % Fe-bearing MgO in good agreement with experiments. Therefore, the broad SCPZ, rendering a smooth change of ferropericlase mechanical properties during the spin crossover, should be mainly caused by entropy, consistent with the high-temperature state of the lower mantle.

DOI: 10.1103/PhysRevB.103.224105

I. INTRODUCTION

Ferropericlase (Fp), the MgO containing ~20 mol % FeO, is believed to be the second most abundant mineral in the Earth's lower mantle (LM) [1]. Its high-pressure (P) properties are critically important for understanding seismological observations related to the LM. Under hydrostatic conditions, Fe^{2+} ions in Fp are located in an octahedral crystal field, which splits fivefold degenerate Fe d orbitals into threefold t_{2g} and twofold e_g degenerate orbitals. At ambient pressure, Fe^{2+} has a high-spin (HS) state, with three (two) d electrons occupying the spin-up t_{2g} (e_g) states and one occupying the spin-down t_{2g} state. Pressurization can transfer two d electrons in the spin-up e_g states into the spin-down t_{2g} states, giving rise to the low-spin (LS) state of Fe^{2+} with empty e_g states, to manifest a pressure-induced HS to LS crossover of Fp. Both experimental measurements [2–20] and theoretical simulations [21–24] have confirmed that the spin crossover in the LM varies with pressure which in turn significantly affects Fp properties [3,6,11,16–18,21,25–27], such as anomalous elasticity variations [16,18,25–27], volume reduction [3,6,21], and partitioning of Fe between Fp and bridgmanite [17]. Consequently, the spin crossover is believed to contribute to the seismic wave heterogeneities in the middle LM, e.g., the steeper-than-normal density gradient in the depth ranging from ~1000 to ~2200 km [28,29].

Based on first-principles calculations and empirical fittings, recent theoretical works have constructed an integrated thermodynamic model of Fe and Al chemistry in the LM conditions [30]. The model demonstrated that the spin crossover of Fe in Fp and Al^{3+} substitution in bridgmanite can induce a chemically stratified LM, consistent with the recent high-resolution tomographic images [30]. Thus, for a better understanding of the LM, the pressure dependence of spin crossover needs to be precisely clarified. But it remains challenging to measure the spin-crossover pressure zone (SCPZ) accurately even at room temperature (T) [2–19], and the experimentally reported values show large variations [see Fig. S1a in Supplemental Material (SM) [31]]. For example, using the optical absorption technique [11], Mössbauer spectroscopy (MBS), [7] and x-ray emission spectroscopy (XES) [12], MgO containing 25 mol % FeO, namely $(Mg_{0.75}Fe_{0.25})O$, was reported to have a different SCPZ of 10, 18, and 24 GPa, respectively.

The SCPZ of Fe-bearing MgO was also extensively investigated by first-principles simulations [21–24,32]. Unfortunately, large discrepancies are found between the experimentally measured [2–20] and theoretically predicted [21–24] room-T SCPZs (Fig. S1 in the SM [31]). One notices that by assuming an ideally periodic Fe substitution in small supercells (containing ~100 atoms), the existing simulations cannot account for the effect of Fe distribution on SCPZs. Even with the inclusion of vibrational entropy effects, the simulation predicted SCPZs (<7GPa) for the ~20 mol % Fe-bearing MgO [21–23] is significantly smaller than the experimental observations (18 GPa [9], 24 GPa [12], and 47 GPa [8]) (Fig. S1b in brown in the SM [31]). On the other

*Corresponding author: xlwang@theory.issp.ac.cn

†Corresponding author: zzeng@theory.issp.ac.cn

hand, a very broad SCPZ, > 70 GPa, was recently reported by simulations considering the mixing enthalpy effects [24] (Fig. S1b in green in the SM [31]), which is notably bigger than the experimental values.

Apparently, the above-mentioned outstanding controversies have to be resolved for a better understanding of SCPZs, and we realize a key missing link lies in the effect of Fe distribution. It is generally accepted that the spin-crossover pressure of Fe in MgO increases with increasing Fe concentration (x) and depends strongly on its local environment [6,8,20,32]. For example, in the supercell with 64 atoms, the predicted spin-crossover pressure of Fe clusters containing two and three Fe ions is 16 and 53 GPa higher than that of one isolated Fe ion, respectively [8]. This behavior can be partially understood by considering the effects of mixing between HS and LS Fe^{2+} as discussed before [24]. Since LS Fe^{2+} (75 pm) has a smaller ionic radius than HS Fe^{2+} (92 pm) and Mg^{2+} (86 pm), the volume of HS Fe-O octahedron next to the LS Fe-O octahedron can expand compared with that next to the Mg-O octahedron [24]. Consequently, the magnetic moments of HS Fe^{2+} next to LS Fe^{2+} can survive pertaining to higher pressure, and this phenomenon will be possibly more pronounced at high Fe concentrations. Therefore, it will be very useful to establish a general relationship between Fe distribution and SCPZ, especially the effect of inhomogeneity in Fe distribution, which can occur over a large length scale that could not be captured by small simulation cells previously employed. Understanding the role of Fe distribution will fill an outstanding gap in our understanding of LM properties, particularly the spin-crossover behaviors of Fe in Fp.

II. METHODS

The first-principles calculations are performed using the Vienna Ab-initio Simulation Package (VASP) [33,34], and the interactions between the core electrons and valence electrons are described by the projector augmented wave (PAW) method [35]. The generalized gradient approximation (GGA) functional of Perdew-Burke-Ernzerhof (PBE) [36] is selected to describe the exchange-correlation energy. The plane wave energy cutoff was set to 550 eV and self-consistent field tolerance is 1.0×10^{-6} eV. The structures are relaxed until the maximum force acting on any atom was less than 1.0×10^{-3} eV/Å. A supercell containing 64 atoms is adopted to investigate the interaction between two Fe ions at static condition, and Brillouin zone is sampled by $6 \times 6 \times 6$ Monkhorst and Pack grid [37]. The formation energy of $(Mg_{0.625}Fe_{0.375})O$ formed by Fe atoms aggregation in 25 and 40 mol % Fe-bearing MgO is calculated by using the supercell with 64 atoms, and the $3 \times 6 \times 4$ Monkhorst and Pack grid is used [37]. To check the reliability of GGA functional for describing the Fe distribution, intense calculations (full structure relaxations and total energy calculations) based on the hybrid functional (HSE06) [38] containing 25% exact exchange contribution, which can give the correct band gap [39], spin-crossover pressure of Fe [40], and configuration of MgO vacancy [41] are carried out, and similar results are obtained (Fig. S3 in the SM [31]). Our test calculations show that for Fe-bearing MgO, GGA can also give comparable lattice constant and high-spin to low-spin-crossover pressure with that of GGA + U, GGA-PBEsol [42], and HSE06 [38].

In order to obtain the phase diagrams of Fe-bearing MgO, it is necessary to search for stable Fe distributions in gigantic supercells by calculating the total energies of a huge number of distribution configurations. However, it is infeasible to carry out such calculations from first principles. Instead, combination of the first-principles method and cluster expansion (CE) method can be an effective approach to tackle this challenging problem, by constructing an Ising-like Hamiltonian to calculating the energy of a huge number of atomic configurations with modest computational cost, as demonstrated in the studies of solid solutions [43].

The effective cluster interaction (ECI) parameters are constructed based on the CE method. In carrying out the progress of CE, all investigated configurations are fully relaxed first by using the first-principles calculations, and the total energies are then expanded with a generalized Ising model, where clusters are expanded in the basis functions of single atoms, pairs, triples, and so on. The expansion formula [44] is shown as

$$E_f = J_0 + \sum_i J_i \sigma_i + \sum_{i<j} J_{ij} \sigma_i \sigma_j + \cdots, \tag{1}$$

where E_f is the formation energy obtained from the first-principles calculations, the indices i and j run over all lattice sites, and σ_m is $+1$ and -1 for Fe and Mg on occupation site m, respectively, and the expansion coefficients J are the ECIs. The accuracy of ECIs are checked by the cross-validation (CV) [45] score as shown in Eq. (2), which is defined as

$$\mathrm{CV} = \left(\frac{1}{n} \sum_{i=1}^{n} (E_i - \hat{E}_i)^2 \right)^{1/2} \tag{2}$$

where E_i and $\hat{E}_i$ are the energies of structure i obtained by using the first-principles calculations and by a least-squares fitting of other $(n-1)$ structural energies, respectively. A smaller CV score indicates more accurate ECI parameters. The score in our simulation is 13.6 meV, much smaller than the widely accepted converged value of 25 meV [45]. Since the pressure loading time is short, we believe that the Fe-distribution features will have marginal changes during the experimental measurements. Therefore, the calculated HS Fe-distribution features at 0 GPa are used for simulating the spin-crossover behaviors.

The semigrand canonical Monte Carlo simulations implemented by the emc2 code [45,46] of the ATAT program [45] are used to obtain the spatial distributions of Fe ions in MgO at temperatures of 300, 600, 900, 1200, 1500, and 1800 K. Supercells constructed by a $36 \times 36 \times 36$ expansion of the primitive cell are used for MC simulations. The initial Fe distributions are randomly generated for each MC simulation. The distribution features are evaluated over 10 000 MC steps/site after 15 000 MC steps/site for equilibration.

III. RESULTS AND DISCUSSION

Using first-principles calculations combined with the cluster expansion (CE) approach and the Monte Carlo (MC)

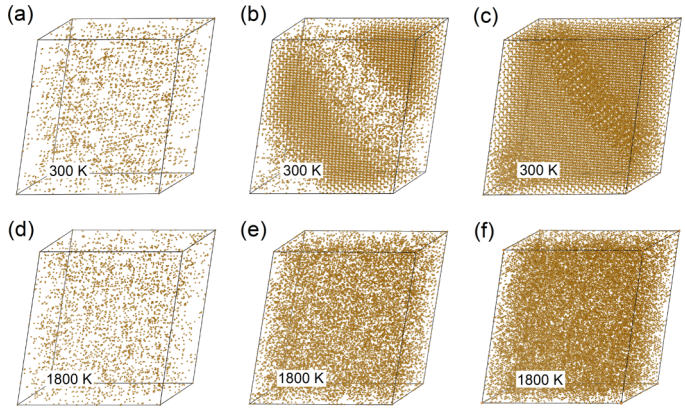

FIG. 1. Snapshots of Fe distributions. The Fe distributions of $(Mg_{0.9375}Fe_{0.0625})O$, $(Mg_{0.75}Fe_{0.25})O$, and $(Mg_{0.6}Fe_{0.4})O$ at 300 K are shown in (a)–(c), respectively, and their counterparts at 1800 K are shown in (d)–(f), respectively. Fe atoms are presented by brown balls, whereas Mg and O atoms are not displayed. At 300 K, in the configurations of $(Mg_{0.75}Fe_{0.25})O$ and $(Mg_{0.6}Fe_{0.4})O$, iron-rich and iron-poor zones can be clearly identified, whereas randomized iron distributions appear at the temperatures of 1800 K. Because the Fe concentration of $(Mg_{0.9375}Fe_{0.0625})O$ is too low, Fe aggregation supposed to occur at 300 K cannot be resolved.

method, we have first investigated the Fe distribution in Fe-bearing MgO as functions of T and x in a large supercell containing 93 312 atoms ($36 \times 36 \times 36$ times the MgO primitive cell). Test calculations with even larger cells, such as the $42 \times 42 \times 42$ (148 176 atoms) supercell were also done to verify the convergence of our simulation results. We found that Fe segregation (clustering) will occur in MgO at temperatures lower than 900 K driven by enthalpy, while the entropy-driven randomized Fe distribution occurs at higher temperature. Then, we studied the effect of Fe distribution on SCPZ. Most notably, the randomized Fe distributions are found to induce broad SCPZs comparable to experimental observations. Thus, in the LM conditions, smooth changes of ferropericlase properties during the spin crossover can be expected by including both iron distribution and temperature effects.

The generally accepted Fe concentration in LM Fp is ~20 mol %, while a composition with higher x, such as $(Mg_{0.6}Fe_{0.4})O$, can also be expected [6]. Therefore, we systematically investigate Fe distributions in MgO with 3.125, 6.25, 12.5, 18, 25, and 40 mol % FeO incorporations. In each case, key features of Fe distribution at temperatures of 300, 600, 900, 1200, 1500, and 1800 K are revealed and analyzed. We note that the Fe-bearing MgO samples are usually synthesized around 1800 K [5,6] approaching to the T (~2000 K) of the upper part of LM [1], where the spin crossover occurs. The snapshots of Fe distribution in the Fe-bearing MgO at 300 and 1800 K after equilibration are shown in Fig. 1 (see also Fig. S2 in the SM [31]). One can clearly see the important effect of temperature on Fe distribution. For sufficiently high Fe concentrations, e.g., 25 mol % [Fig. 1(b)], 40 mol % [Fig. 1(c)], and also 18 mol % (Fig. S2c in the SM [31]), Fe segregation (i.e., MgO and FeO phase separation) occurs at low temperature of 300 K, while a homogeneous phase occurs at high temperature of 1800 K. We note that in principle, Fe segregation should also occur for low Fe concentrations at 300 K, but the amount of Fe-rich phase is too small to be seen in Fig. 1(a) for $(Mg_{0.9375}Fe_{0.0625})O$ [see also Fig. S3a in the SM [31] for $(Mg_{0.96875}Fe_{0.03125})O$] and slight Fe aggregation can be seen in 12.5 mol % Fe-bearing MgO (Fig. S2b in the SM [31]) at 300 K. These results indicate that for the Fe concentrations of geophysical interest (20–40 mol %), iron in Fe-bearing MgO tends to cluster at low temperature, which is consistent with our static calculations (Fig. S3 in the SM [31]). The Fe segregation occurs also at 600 K (Fig. S4 in the SM [31]). This is simply because at low temperature, the enthalpy contribution (as reflected from the calculated clustering energy) dominates over the entropy contribution ($-TS_{\text{conf}}$, where S_{conf} is the configuration entropy), while the reverse is true at high temperature where the entropy-driven randomized Fe distributions occur at 1800 K for all the Fe concentrations. We have estimated from simulations that the critical temperature for phase segregation is ~900 K (Fig. S4 in the SM [31]), which is in reasonably good agreement with the thermodynamic phase diagram [47].

To further quantify the Fe distributions shown in Fig. 1 and reveal their effects on the spin-crossover behaviors of Fe, the simulated system with 93 312 atoms is divided into 729 cubic segments containing 64 cation and anion sites, and a schematic view of the segmentation is shown in Fig. S5 (in the SM [31]). For 6.25, 25, and 40 mol % Fe-bearing MgO, the number of segments containing the same number of Fe atoms (or with the same local Fe concentration, hereafter named x_{loc}) are counted. The results are shown in the histogram plot in Fig. 2 using the upper X axis, to quantify the distribution of local Fe concentration. At a low temperature of 300 K, the histograms in Figs. 2(b) and 2(c) show apparently a bimodal Fe distribution, which is fit with two Gaussian functions. The two peak positions are located one above and one below the nominal Fe concentration of 25 and 40 mol % in Figs. 2(b) and 2(c), respectively, indicating phase segregation into one Fe-rich and one Fe-poor phase. For the very low Fe concentration of 6.25 mol % shown in Fig. 2(a), there should be two distributions in principle, but only the Fe-poor peak can be seen, while the Fe-rich peak could not show up because of too small an amount. As shown in Figs. 2(b) and 2(c), a sharp peak at $x_{\text{loc}} = 0.375$ can be seen in the 25 and 40/mol % Fe-bearing MgO at 300 K, and the Fe atoms tend to segregate to the phase with 37.5 mol % FeO substitution, which has a periodic Fe distribution (Fig. S6 and Table S1 in the SM [31]). The calculated formation energy of the phase with 37.5 mol % FeO substitution is negative indicating that it is energetically stable (Fig. S6 in the SM [31]). In contrast, at high temperature of 1800 K, the histograms in Figs. 2(b) and 2(c) exhibit a monodistribution, which can be nicely fit by one Gaussian function with the peak position coinciding perfectly with their respective nominal Fe concentration, i.e., the fit peak positions of $(Mg_{0.75}Fe_{0.25})O$ and $(Mg_{0.6}Fe_{0.4})O$ at 0.247 and 0.401, respectively. Generally, our results show that above 900 K, the Fe distributions can be fit well by one normal Gaussian function, indicating a homogeneous random Fe distribution. Similar results are also obtained using smaller segments containing 32 cation and anion sites (Fig. S7 in the SM [31]).

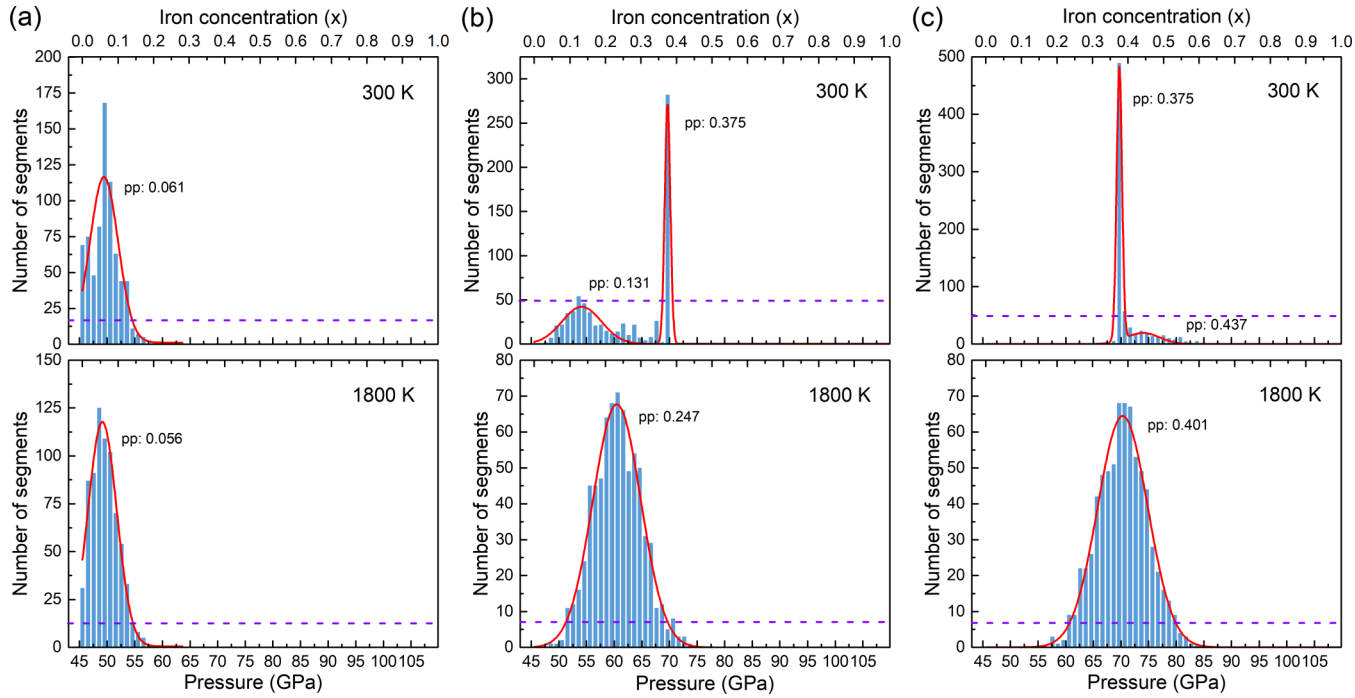

FIG. 2. Histograms showing the number of segments with the same local iron concentration and the same spin-crossover pressure. (a)–(c) Results of $(Mg_{0.9375}Fe_{0.0625})$, $(Mg_{0.75}Fe_{0.25})O$, and $(Mg_{0.6}Fe_{0.4})O$, respectively. The upper X axis (lower X axis) presents the segments distribution feature with local iron concentration (spin-crossover pressure). The segments containing 64 cation sites and 64 anion sites are used. Red lines are the results of Gaussian fittings. Bimodal and mono Gaussian fittings are used for the configurations with and without Fe enrichments, respectively, and the fitted peak positions (pp) are indicated next to the peaks. The purple-dashed line represents the assumed detectable critical number of 10% of the highest histogram bar.

Next, we discuss the effects of Fe distribution on the spin-crossover behavior. Since experimental observations clearly showed that the spin-crossover pressure of Fe in MgO increases with increasing x (Fig. S1a in the SM [31]), a linear function, $P(x) = 64.3x + 45.5$ (red line in Fig. S1a in the SM [31]), is obtained by fitting experimental results. Correspondingly, the divided segments with higher local Fe concentrations will have higher "local" spin-crossover pressures. For example, the segments with x_{loc} of 0.1 and 0.25 will have the spin-crossover pressures of 51.9 and 61.6 GPa, respectively. In the lower X axis of the histogram plot in Fig. 2, the number of segments with the same spin-crossover pressure are counted and shown. Then, we determine the SCPZs at 300 and 1800 K, respectively, by assuming a detection limit of 10% of the highest histogram bar. This means the spin crossover of any given segment cannot be detected below this limit, which is shown by the dashed purple lines in Fig. 2, and our main conclusion would not be altered by this assumption. Based on the SCPZs of all investigated iron concentrations, a linear interpolation is used to calculate the SCPZs of MgO incorporated with 3.125–40 mol % FeO, which are summarized in the phase diagram, as constructed in Fig. 3 (1800 K) and Fig. S8 (300 K, in the SM [31]).

A broad SCPZ is induced by the Fe distribution at 1800 K (Figs. 2 and 3). Specifically, the simulated SCPZ of MgO incorporated with 18 and 25 mol % Fe is 14.9 and 17.5 GPa, respectively, while it reaches the maximum of 19.1 GPa in the case of $x = 0.37$. These SCPZ values agree well with the experimental observations [2–20]. For example, the predicted value of 17.5 GPa for 25 mol % FeO incorporated in MgO is generally consistent with the measured experimental range 10–24 GPa [7,11,12]. These results show that the high-T entropy-broadened Fe distribution, having large local

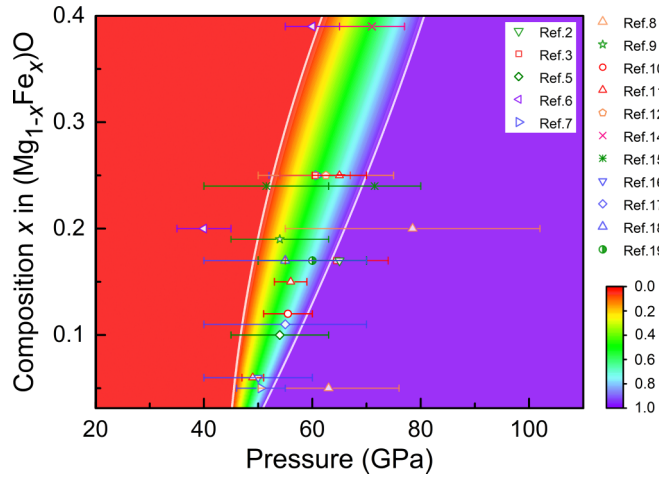

FIG. 3. Low-spin Fe fractions and phase diagram. The fraction of LS iron in Fe-bearing MgO is shown as functions of pressure and iron concentration. Red zone and violet zone show Fe in the HS and LS state, respectively. The area located between two white solid lines presents the coexisting zone of HS and LS Fe. Experimental results at room temperature are shown in horizontal bars. The simulated spin-crossover pressure zones agree well with experimental ones.

concentration variations, is the dominant factor in determining the SCPZ of Fe in MgO. Correspondingly, along the LM geotherm, the entropy-broadened Fe distribution will also contribute notably to the SCPZ. Previous theoretical investigations [21–24] indicated that about 50 GPa SCPZ can be caused by the mixing enthalpy or entropy effects in Fe-bearing MgO under ∼2000 K. Together with the broad SCPZ induced by Fe distribution, 15–19 GPa, one could therefore expect a continuous and smooth change of Fe spin state in Fp under LM conditions. Consequently, the spin-crossover induced changes of Fp properties should also occur in a much broader range due to the effects of Fe distribution.

Differing from the broad and continuous SCPZ induced by homogeneous Fe distribution at high T (Fig. 3), phase segregation occurs at 300 K and the resulting SCPZs of 25 and 40 mol % Fe-bearing MgO are very narrow, as shown in Fig. 2(b) and Fig. S8 (in the SM [31]). Specifically, a two-step spin-crossover behavior is found in the case of 25 mol % Fe-bearing MgO. Such narrow SCPZs are obviously different from the experimentally observed broad and smooth SCPZs (Fig. S8 in the SM [31]). This indicates that the experimental samples should contain little Fe segregation. This is reasonable, since the Fe-bearing MgO samples are synthesized first at high T by using laser heating [5,6] and subsequently quenched to low T, and the experimentally reported diffusion rates of iron in Fp will decrease drastically as T decreases [48,49]. Consequently, the high-T Fe distributions are expected to be largely frozen-in in the samples at low T where the measurements were conducted.

IV. CONCLUSION

In summary, the effect of Fe distribution in ferropericlase have been systematically investigated as functions of temperature and Fe concentration, most notably in large supercells with $\sim 10^6$ atoms, which reveals an entropy-driven transition from segregated to randomized Fe distribution occurring at ∼900 K. The randomization of Fe distribution is then found to play a key role in broadening the spin-crossover pressure zone that agrees with the experimentally observed ranges. Consequently, in the lower mantle, similar entropy-driven broad spin-crossover pressure zones are expected, which in turn give rise to smooth changes of ferropericlase properties during the spin crossover. Furthermore, since properties of materials are sensitive to their microstructure, Fe distribution may also play an important role in affecting the melting temperature, thermal conductivity, and electrical conductivity of ferropericlase. Meanwhile, the effects of impurity distribution should also be taken seriously when exploring the properties of other minerals, e.g., FeAl-bearing $MgSiO_3$ bridgmanite. Generally, the knowledge we learned here can also be transferred to better understanding the properties of transition metal compounds under high P, and our theoretical methods can be applied to studying high-pressure properties of diluted magnetic solid solutions containing transition metal elements.

ACKNOWLEDGMENTS

This work was supported by the National Natural Science Foundation of China (Grant No. 11674329), NSAF (Grants No. U1230202 and No. U2030114), and Science Challenge Project (Grant No. TZ2016001). The calculations were partly performed in the Center for Computational Science of CASHIPS, the ScGrid of Supercomputing Center and Computer Network Information Center of Chinese Academy of Sciences, and partly using a Tianhe-2JK computing time award at the Beijing Computational Science Research Center (CSRC). The authors also acknowledge F. Liu, A. Goncharov and A. Metsue for helpful discussions.

Author contributions are as follows: X.W.: conceptualization, methodology, formal analysis, original draft preparation; K.Y.: investigation, methodology, software, data curation, formal analysis, visualization; J.Z., Y.C., C.Z., and H.L.: resources, project administration, validation, formal analysis; X.W. and Z.Z.: supervision, funding acquisition, reviewing, editing.

[1] J.-P. Poirier, *Introduction to the Physics of the Earth's Interrior* (Cambridge University Press, Cambridge, UK, 1991).
[2] J. Badro, G. Fiquet, F. Guyot, J.-P. Rueff, V. V. Struzhkin, G. Vankó, and G. Monaco, Science **300**, 789 (2003).
[3] J. F. Lin, V. V. Struzhkin, S. D. Jacobsen, M. Y. Hu, P. Chow, J. Kung, H. Liu, H.-k. Mao, and R. J. Hemley, Nature (London) **436**, 377 (2005).
[4] M. P. Pasternak, R. D. Taylor, R. Jeanloz, X. Li, J. H. Nguyen, and C. A. McCammon, Phys. Rev. Lett. **79**, 5046 (1997).
[5] H. Marquardt, S. Speziale, H. J. Reichmann, D. J. Frost, and F. R. Schilling, Earth Planet. Sci. Lett. **287**, 345 (2009).
[6] Y. Fei, L. Zhang, A. Corgne, H. Watson, A. Ricolleau, Y. Meng, and V. Prakapenka, Geophys. Res. Lett. **34**, L17307 (2007).
[7] J. F. Lin, A. G. Gavriliuk, V. V. Struzhkin, S. D. Jacobsen, W. Sturhahn, M. Y. Hu, P. Chow, and C.-S. Yoo, Phys. Rev. B **73**, 113107 (2006).
[8] I. Kantor, L. Dubrovinsky, C. McCammon, G. Steinle-Neumann, A. Kantor, N. Skorodumova, S. Pascarelli, and G. Aquilanti, Phys. Rev. B **80**, 014204 (2009).
[9] T. Komabayashi, K. Hirose, Y. Nagaya, E. Sugimura, and Y. Ohishi, Earth Planet. Sci. Lett. **297**, 691 (2010).
[10] H. Keppler, I. Kantor, and L. S. Dubrovinsky, Am. Mineral. **92**, 433 (2007).
[11] A. F. Goncharov, V. V. Struzhkin, and S. D. Jacobsen, Science **312**, 1205 (2006).
[12] Z. Mao, J.-F. Lin, J. Liu, and V. B. Prakapenka, Geophys. Res. Lett. **38**, L23308 (2011).
[13] B. Chen, J. M. Jackson, W. Sturhahn, D. Zhang, J. Zhao, J. K. Wicks, and C. A. Murphy, J. Geophys. Res. **117**, B08208 (2012).
[14] K. K. Zhuravlev, J. M. Jackson, A. S. Wolf, J. K. Wicks, J. Yan, and S. M. Clark, Phys. Chem. Miner. **37**, 465 (2010).
[15] K. Glazyrin, N. Miyajima, J. S. Smith, and K. K. M. Lee, J. Geophys. Res. **121**, 3377 (2016).
[16] J. C. Crowhurst, J. M. Brown, A. F. Goncharov, and S. D. Jacobsen, Science **319**, 451 (2008).
[17] T. Irifune, T. Shinmei, C. A. McCammon, N. Miyajima, D. C. Rubie, and D. J. Frost, Science **327**, 193 (2010).

[18] D. Antonangeli, S. J, C. M. Aracne, D. L. Farber, A. Bosak, M. Hoesch, M. Krisch, F. J. Ryerson, G. Fiquet, and J. Badro, Science **331**, 64 (2011).
[19] E. Ito, T. Yoshino, D. Yamazaki, A. S. Shatskiy, S. Shan, X. Guo, T. Katsura, Y. Higo, and K. Funakoshi, J. Phys. Conf. Ser. **215**, 012099 (2010).
[20] S. Speziale, A. Milner, V. E. Lee, S. M. Clark, M. P. Pasternak, and R. Jeanloz, Proc. Natl. Acad. Sci. USA **102**, 17918 (2005).
[21] T. Tsuchiya, R. M. Wentzcovitch, C. R. S. da Silva, and S. de Gironcoli, Phys. Rev. Lett. **96**, 198501 (2006).
[22] Z. Wu and R. M. Wentzcovitch, Proc. Natl. Acad. Sci. USA **111**, 10468 (2014).
[23] R. M. Wentzcovitch, J. F. Justo, Z. Wu, C. R. da Silva, D. A. Yuen, and D. Kohlstedt, Proc. Natl. Acad. Sci. USA **106**, 8447 (2009).
[24] E. Holmström and L. Stixrude, Phys. Rev. Lett. **114**, 117202 (2015).
[25] H. Marquardt, S. Speziale, H. J. Reichmann, D. J. Frost, F. R. Schilling, and E. J. Garnero, Science **324**, 224 (2009).
[26] M. Murakami, Y. Ohishi, N. Hirao, and K. Hirose, Nature (London) **485**, 90 (2012).
[27] Z. Wu, J. F. Justo, and R. M. Wentzcovitch, Phys. Rev. Lett. **110**, 228501 (2013).
[28] L. H. Kellogg, B. H. Hager, and R. D. van der Hilst, Science **283**, 1881 (1999).
[29] J. Trampert, F. Deschamps, J. Resovsky, and D. Yuen, Science **306**, 853 (2004).
[30] S. Xu, J.-F. Lin, and D. Morgan, J. Geophys. Res. **122**, 1074 (2017).
[31] See Supplemental Material at http://link.aps.org/supplemental/10.1103/PhysRevB.103.224105 which contains Refs. [50,51], a summary of reported experimentally measured Fe spin-crossover pressure zones in Fp, snapshots of $(Mg_{1-x}Fe_x)O$ ($x = 0.031\,25, 0.125, 0.18$), total energies as a function of distance between two Fe atoms, low-spin Fe fractions and phase diagram of $(Mg_{1-x}Fe_x)O$ at 300 K, and crystallographic parameters of $(Mg_{0.625}Fe_{0.375})O$ phase.
[32] K. Persson, A. Bengtson, G. Ceder, and D. Morgan, Geophys. Res. Lett. **33**, L16306 (2006).
[33] G. Kresse and J. Furthmüller, Comput. Mater. Sci. **6**, 15 (1996).
[34] G. Kresse and J. Furthmüller, Phys. Rev. B **54**, 11169 (1996).
[35] G. Kresse and D. Joubert, Phys. Rev. B **59**, 1758 (1999).
[36] J. P. Perdew, K. Burke, and M. Ernzerhof, Phys. Rev. Lett. **77**, 3865 (1996).
[37] H. J. Monkhorst and J. D. Pack, Phys. Rev. B **13**, 5188 (1976).
[38] A. V. Krukau, O. A. Vydrov, A. F. Izmaylov, and G. E. Scuseria, J. Chem. Phys. **125**, 224106 (2006).
[39] M. Marsman, J. Paier, A. Stroppa, and G. Kresse, J. Phys.: Condens. Matter **20**, 064201 (2008).
[40] M. Alfredsson, J. P. Brodholt, P. B. Wilson, G. D. Price, F. Corà, M. Calleja, R. Bruin, L. J. Blanshard, and R. P. Tyer, Model. Simul. **31**, 367 (2005).
[41] A. Droghetti, C. D. Pemmaraju, and S. Sanvito, Phys. Rev. B **81**, 092403 (2010).
[42] L. Schimka, J. Harl, and G. Kresse, J. Chem. Phys. **134**, 024116 (2011).
[43] C. D. R. Ludwig, T. Gruhn, C. Felser, T. Schilling, J. Windeln, and P. Kratzer, Phys. Rev. Lett. **105**, 025702 (2010).
[44] J. M. Sanchez, F. Ducastelle, and D. Gratias, Phys. A (Amsterdam, Neth.) **128**, 334 (1984).
[45] A. van de Walle, M. Asta, and G. Ceder, Calphad **26**, 539 (2002).
[46] A. van de Walle and M. Asta, Modell. Simul. Mater. Sci. Eng. **10**, 521 (2002).
[47] https://www.crct.polymtl.ca/fact/phase_diagram.php?file=FeO-MgO.jpg&dir=TDnucl.
[48] D. Yamazaki and T. Irifune, Earth Planet. Sci. Lett. **216**, 301 (2003).
[49] M. W. Ammann, J. P. Brodholt, and D. P. Dobson, Earth Planet. Sci. Lett. **302**, 393 (2011).
[50] I. S. Lyubutin, V. V. Struzhkin, A. A. Mironovich, A. G. Gavriliuk, P. G. Naumov, J. F. Lin, and R. J. Hemley, Proc. Natl. Acad. Sci. USA **110**, 7142 (2013).
[51] J. Badro, V. V. Struzhkin, J. Shu, R. J. Hemley, H. K. Mao, C. C. Kao, J. P. Rueff, and G. Shen, Phys. Rev. Lett. **83**, 4101 (1999).